



Article

Rare earth mineral diversity controlled by REE pattern shapes

Michael Anenburg*

Research School of Earth Sciences, Australian National University, Canberra, ACT 2600, Australia.

Abstract

The line connecting rare earth elements (REE) in chondrite-normalised plots can be represented by a smooth polynomial function using λ shape coefficients as described by O'Neill (2016). In this study, computationally generated λ combinations are used to construct artificial chondrite-normalised REE patterns that encompass most REE patterns likely to occur in natural materials. The dominant REE per pattern is identified, which would lead to its inclusion in a hypothetical mineral suffix, had this mineral contained essential REE. Furthermore, negative Ce and Y anomalies, common in natural minerals, are considered in the modelled REE patterns to investigate the effect of their exclusion on the relative abundance of the remainder REE. The dominant REE in a mineral results from distinct pattern shapes requiring specific fractionation processes, thus providing information on its genesis. Minerals dominated by heavy lanthanides are rare or non-existent, even though the present analysis shows that REE patterns dominated by Gd, Dy, Er and Yb are geologically plausible. This discrepancy is caused by the inclusion of Y, which dominates heavy REE budgets, in mineral name suffixes. The focus on Y obscures heavy lanthanide mineral diversity and can lead to various fractionation processes to be overlooked. Samarium dominant minerals are known, even though deemed unlikely by the computational model, suggesting additional fractionation processes that are not well described by λ shape coefficients. Positive Eu anomalies only need to be moderate in minerals depleted in the light REE for Eu to be the dominant REE, thus identifying candidate rocks in which the first Eu dominant mineral might be found. Here, I present an online tool, called *ALambdaR* that allows interactive control of λ shape coefficients and visualisation of resulting REE patterns.

Keywords: rare earth elements, mineral evolution, lambda shape coefficients, europium anomaly, cerium anomaly, orthogonal polynomials, lanthanides, normalisation

(Received 24 April 2020; accepted 8 September 2020; Accepted Manuscript published online: 11 September 2020; Associate Editor: Koichi Momma)

Introduction

Overview of REE patterns

The series of elements from La through to Lu are known as the lanthanides. Under typical geological conditions they occur as trivalent cations with the exception of Ce (also often tetravalent) and Eu (often also divalent). Their valence electron structures are similar, and cationic radii vary quadratically from the large La^{3+} to the small Lu^{3+} due to the lanthanide contraction (Raymond *et al.*, 2010; Seitz *et al.*, 2007). This contraction, together with its effect on mesoscale molecular interactions (Ferru *et al.*, 2016) leads to small yet gradual and predictable changes in their chemical behaviour. Yttrium is positioned above the lanthanides in group 3 of the periodic table, and it often behaves like Dy or Ho, particularly in high-temperature igneous or metamorphic environments (Pack *et al.*, 2007). The lanthanides and Y, excluding the unstable Pm (whose natural abundance is negligible, Kuroda, 1982), are often grouped together as the rare earth elements (REE: Balaram, 2019; Cheisson and Schelter, 2019). Subsets of the REE group that commonly occur together in various rocks and minerals are termed as the light REE (LREE), heavy REE (HREE), and less commonly, the middle REE (MREE), with the exact boundaries between the subsets varying between

authors. Often, the LREE group includes La to Sm, whereas the HREE group includes Eu to Lu. The MREE group, when used, typically includes Sm to Dy. The smooth variation in the chemical properties between the REE allows systematic fractionation from each other, and studies into these processes provide windows into a variety of geochemical and cosmochemical processes.

Although differences between the REE chemical properties are gradual, the variation in their natural abundances is not. They follow the Oddo–Harkins rule, which states that elements with even atomic numbers (e.g. Dy) are more abundant than their neighbouring odd-numbered elements (e.g. Tb and Ho) (Harkins, 1917; Palme *et al.*, 2014). This complicates comparison of subtle differences between rocks or minerals because of the characteristic zig-zag shape of REE abundance plots (Taylor, 1962). The difficulty is resolved by normalisation to REE contents of a representative primitive or primordial reservoir, most commonly CI chondrites (Coryell *et al.*, 1963). When plotted in a logarithmic scale, the normalisation results in generally smooth REE patterns in which fractionation trends become obvious, facilitating the use of REE patterns as petrogenetic tools.

A practical limitation stems from the appearance of each analysis as a line on REE plots, which convolutes studies of large analytical data sets owing to visual overload. O'Neill (2016) developed a method to represent REE patterns by the polynomial:

$$\ln\left(\frac{[\text{REE}]}{[\text{REE}]_{\text{CI}}}\right) = \lambda_0 + \lambda_1 f_1 + \lambda_2 f_2 + \dots,$$

*Author for correspondence: Michael Anenburg, Email: michael.anenburg@anu.edu.au
Cite this article: Anenburg M. (2020) Rare earth mineral diversity controlled by REE pattern shapes. *Mineralogical Magazine* 84, 629–639. <https://doi.org/10.1180/mgm.2020.70>

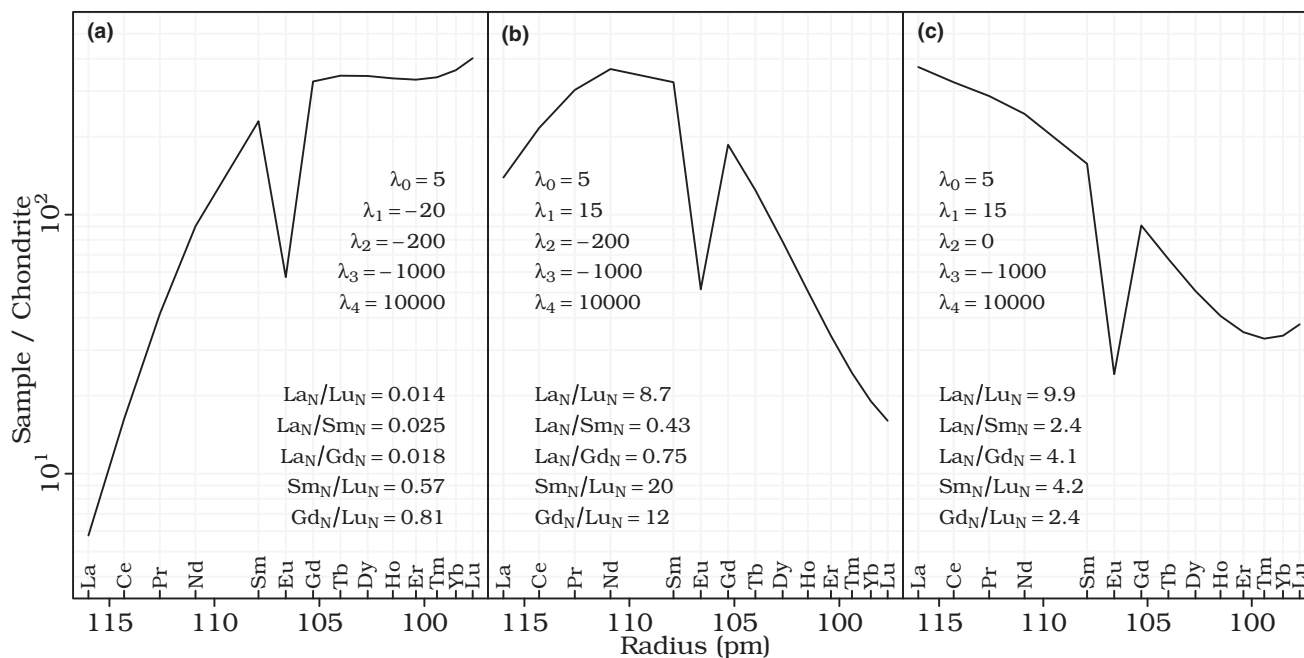


Fig. 1. Three different REE patterns generated from a set of λ coefficients and Eu anomaly set at 0.2. Chondrite-normalised element ratios are calculated for each pattern and annotated on the figure.

where $[REE]$ and $[REE]_{CI}$ are measured and chondritic abundance of each REE, respectively, λ_n are shape coefficients, and f_n are precalculated orthogonal polynomials in r_{VII}^{3+} , the ionic radius of trivalent cations in eight-fold coordination from Shannon (1976) for each respective REE. The orthogonality of the polynomials ensures that the shape coefficients are independent of each other so that, for example, truncating the polynomial series at $\lambda_n f_n$ does not affect the values of λ_{n-1} etc. The process of deriving λ shape coefficients from a REE pattern can be achieved using dedicated software such as the spreadsheet available in the Supplementary data of O'Neill (2016), or the Python package 'pyrolite' (Williams *et al.*, 2020). Most REE patterns can be closely reproduced by three to four shape coefficients, where the physical significance of λ_0 is the overall abundance of the REE, λ_1 is the linear slope, λ_2 is the quadratic curvature and λ_3 represents the inflections at the ends of patterns (sinusoidality). Rarely, a fifth λ_4 term is required if any 'W' shape is present in the pattern. Representation of REE patterns by their λ shape coefficients reduces the dimension of each analysis from a line to a point that can be plotted in λ -space. Often, λ_2 - λ_1 plots (quadratic curvature versus slope) are the most instructive (O'Neill, 2016).

Quantitative description of REE pattern shapes

The merit of using λ shape coefficients instead of other pattern shape indicators is now discussed. Various shape aspects of REE patterns are often described quantitatively with normalised element ratios (denoted by subscript N). For example, La_N/Lu_N is a measure of the overall slope of the pattern, whereas La_N/Sm_N might be a measure of the LREE enrichment of a pattern. However, these ratios fail to capture some of the complexities that often occur in patterns, such as curvature or sinusoidality. When ratios are used, the choice of elements is often arbitrary, with some workers choosing Ce over La, Nd or Gd over Sm, and Yb over Lu. This inconsistency can lead to biases depending

on the hypothesis in discussion, as these diagrams are plotted on logarithmic scales and small distances in the vertical scale often translate to large differences in element ratios. Finally, these ratios are not independent of each other. This problem is illustrated in Fig. 1. Garnets, for example, commonly have REE patterns with strongly depleted LREE contents which steeply rise towards the MREE, and the HREE are usually sub-horizontal. The REE pattern generated from λ values shown in Fig. 1a is an example of such a garnet-like pattern. Several normalised element ratios are calculated in order to provide information on the shape. La_N/Lu_N , Sm_N and Gd_N are small numbers, confirming the overall strongly positive slope of the pattern. Sm_N/Lu_N and Gd_N/Lu_N are close to unity, reflecting the flattening of the HREE. Rare earth element patterns for garnets often exhibit their inflection point at Eu, which would make it an ideal element to use in ratios. However, due to the redox behaviour of Eu it occasionally shows negative or positive anomalies, rendering it useless for this purpose. The pattern in Fig. 1a is then rotated clockwise by increasing λ_1 from -20 to 15, while the terms describing curvature (λ_2 to λ_4) remain fixed, leading to the expected increase of La_N/Lu_N (Fig. 1b). However, all other ratios shown in Fig. 1b also increase by more than an order of magnitude. If the purpose of ratios (i.e. those involving Sm and Gd) is to provide some information about the curvature (e.g. Davidson *et al.*, 2013), then they clearly fail because the curvature has not been modified. Additionally, it is now difficult to infer from these ratios that the HREE line is nearly straight. The correlation between normalised elemental ratios increases the challenges for their interpretation when the variation between REE patterns includes more than just the slope. Fig. 1c shows the pattern from Fig. 1b, but with the quadratic curvature term eliminated (i.e. $\lambda = 0$). La_N/Lu_N and La_N/Gd_N increase whereas Sm_N/Lu_N and Gd_N/Lu_N decrease. These changes are reversed in positively sloping patterns (i.e. $La_N/Lu_N < 0$), even though the change in quadratic curvature is identical. Consequently, these ratios become meaningless in

many cases, for instance in analyses of rock suites containing both positively and negatively sloping REE patterns. Methods of measuring curvature by interpolation (e.g. Dy/Dy^* , Davidson *et al.*, 2013) are likewise not independent and can be compromised by other shape features in a pattern (e.g. sinusoidality). Additional applications of the λ method are described by O'Neill (2016). As the method is new and not yet widely adopted, it may be difficult to understand intuitively and visualise how each λ coefficient affects the shape of the REE patterns. This article is accompanied by an interactive online app (*ALambdaR*), briefly described in the Appendix, which allows independent experimentation with construction of REE patterns from λ shape coefficients.

Artificial REE patterns

O'Neill (2016) originally intended for the λ shape coefficients to be used as a tool for interpretation of natural REE patterns. However, as mentioned above, the shape coefficients are orthogonal and not correlated with each other. This means that each shape coefficient can be varied independently, allowing one shape component of a pattern (e.g. curvature) to vary while others (e.g. slope and sinusoidality) remain fixed. This property can be used to construct artificial REE patterns that cover all possible REE patterns representable by the λ shape coefficients. These include a large proportion of all smoothly-varying REE patterns in Nature.

In this study I show how artificial REE patterns are constructed. A simple application is demonstrated, whereby the most abundant REE in a pattern is identified as a function of the λ shape coefficients. As the most abundant REE gives its name to a rare earth mineral via the Levinson suffix, this study has implications for prediction of yet unknown mineral species and mineral evolution, and it provides an example of the data-driven abductive approach to mineralogy (Hazen, 2014). The two most common REEs, Ce and Y, can also behave anomalously under certain conditions. The effect of their removal is examined in this study.

Methods

A script using the R programming language was written to generate REE patterns from combinations of λ shape coefficients (available in the Supplementary data, with a mathematical treatment of the process available in the Appendix). A graphical user interface is provided in the accompanying online app (*ALambdaR*) to simplify and automate the processes and readers are encouraged to experiment with the effect of various λ coefficient combinations.

In this study, only the overall pattern shape is of importance, and therefore λ_0 can be neglected as it merely shifts a pattern up or down on a chondrite-normalised plot. Only two variables can be easily conveyed in 2D plots. Consequently, the slope and curvature coefficients are used as the horizontal and vertical axes, and cover the ranges $\lambda_2 = [-750, 750]$ and $\lambda_3 = [-6500, 6500]$ at intervals of 4 and 40, respectively. The other coefficients are fixed at $\lambda_1 = \{-25, -17, -12, -9, -7, -5, -3, 0, 5, 15\}$ and $\lambda_4 = \{-40,000, 0, 40,000\}$, with each combination shown by a single panel in the following plots.

A total of $10 \times 376 \times 326 \times 3 = 3,677,280$ unique REE patterns were generated. Yttrium is added to each pattern according to a chondritic $Y/Ho = 25.5$. Next, the most abundant REE on an atomic basis is identified for each pattern, and the ratio between

that element and Eu is calculated. This process is repeated while disregarding Ce and Y to account for possible negative anomalies.

Results and discussion

The range of different REE patterns generated in this study is shown in Fig. 2. Each panel represents a combination of single λ_1 and λ_4 , and range of λ_2 and λ_3 values. Representative REE patterns are plotted in their respective positions in the panels. The reader is encouraged to recreate the patterns using the accompanying online app (*ALambdaR*) to better appreciate the λ concept. A careful examination of how patterns vary with λ_1 to λ_4 allows one to intuitively grasp the meaning of each shape coefficient and how they interact when combined linearly. Those who have worked with REE before will soon recognise that many natural patterns (excepting Ce or Eu anomalies) closely resemble the patterns in Fig. 2, particularly at $\lambda = 0$. Conversely, some extreme values such as those at $\lambda_2 > 500$ are probably unrealistic. Generally speaking, patterns at and around the centre are the most likely patterns that appear in Nature due to the largely systematic variation between neighbouring REE described by λ_2 and λ_3 close to zero.

The most abundant REE on an atomic basis in a pattern are depicted in Fig. 3. The pattern can be seen by recreating it in the online app, or by referring back to the same λ -coordinates in Fig. 2. The respective point on each panel is then coloured according to the most abundant REE. As similar patterns result from similar REE contents, the most abundant REE form similarly-coloured regions which encompass REE pattern families. For example, the labelled panel in Fig. 3i shows four regions, each dominated by La, Ce, Nd and Y. By comparing it with its respective panel in Fig. 2s, it can be seen that: (1) the rightmost La-dominated part of the panel indeed contains REE patterns with strong La enrichments; (2) the bottom-right Ce-dominated part of the panel contains REE patterns with LREE enrichment but an inflection point that lowers La contents relative to Ce; (3) the bottom Nd-dominated part of the panel corresponds with patterns strongly enriched in the lighter MREE; and (4) the Y-dominated remainder consists of all other patterns.

The predominant REE in each pattern strongly depends on whether Y and Ce are present. When included in the calculation, negatively sloping patterns (i.e. $\lambda_1 < 0$) are dominated by Y, with some Yb in the unrealistically high- λ_2 -low- λ_3 cases (Fig. 3). As the patterns flatten and then begin to slope positively (i.e. $\lambda_1 \geq 0$), the dominance of La, Ce and Nd expands at the expense of Y and Yb.

Rare earth element patterns of most crustal rocks are either weakly positively sloping or negatively sloping (i.e. $-5 \leq \lambda_2 \leq 15$, Fig. 2), have little curvature or sinusoidality (i.e. would plot close to the centre of each panel), with negligible Ce and Y anomalies (O'Neill, 2016). The second row of Fig. 3 (f-j) shows that these patterns are dominated by either Y or Ce. This is in perfect agreement with currently known REE minerals, and a consequence of their crustal abundance, with Ce being the most abundant LREE at $63 \mu\text{g g}^{-1}$ and Y being the most abundant HREE at $21 \mu\text{g g}^{-1}$ (Rudnick and Gao, 2014). There are 112 Y minerals (i.e. REE-essential minerals dominated by Y) and 137 Ce minerals, which together account for 75.7% out of all IMA-approved REE minerals (see McLeod and Shaulis, 2018 for an analysis of REE mineral occurrences). These two are followed by La (46 minerals, or 14.0%), Nd (27, or 8.2%) and Yb (4, or

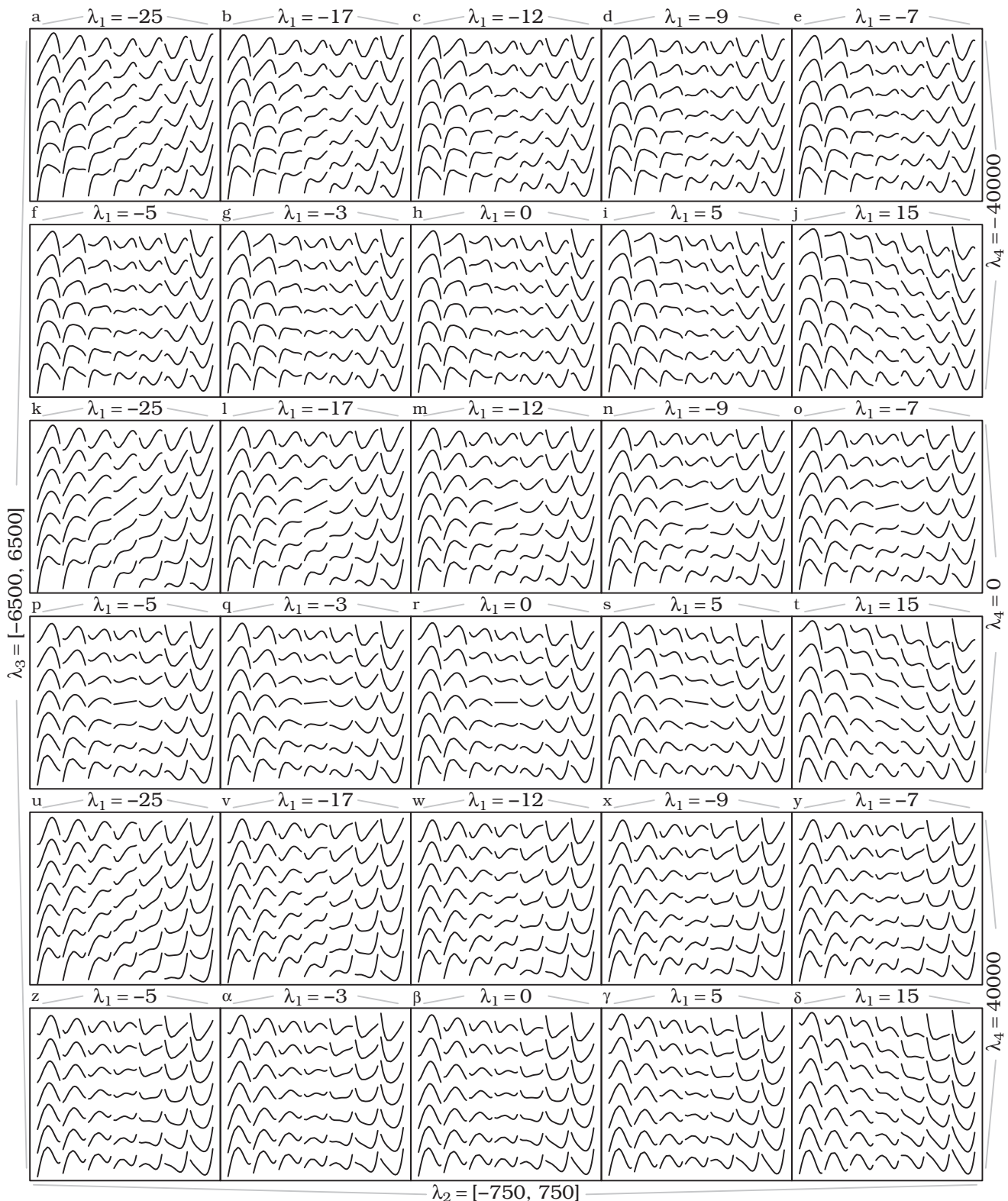


Fig. 2. A representative example of REE patterns, drawn in a qualitative but consistent scale. Each panel has discrete λ_1 and λ_4 indicated by the annotation above each panel and on the right side. Within each panel, the horizontal axis covers $\lambda_2 = [-750, 750]$, and the vertical axis covers $\lambda_3 = [-6500, 6500]$. λ_2 and λ_3 are 0 at the centre of each panel.

1.2%). The \sim factor-of-two predominance of La over Nd minerals is puzzling, as their crustal abundances are similar (La at $31 \mu\text{g g}^{-1}$ and Nd at $27 \mu\text{g g}^{-1}$) (Rudnick and Gao, 2014), and the La field is

located at the right-hand side of each panel in Fig. 3, which was described above as less likely to occur in natural rocks. This issue can be resolved if negative Ce anomalies are considered.

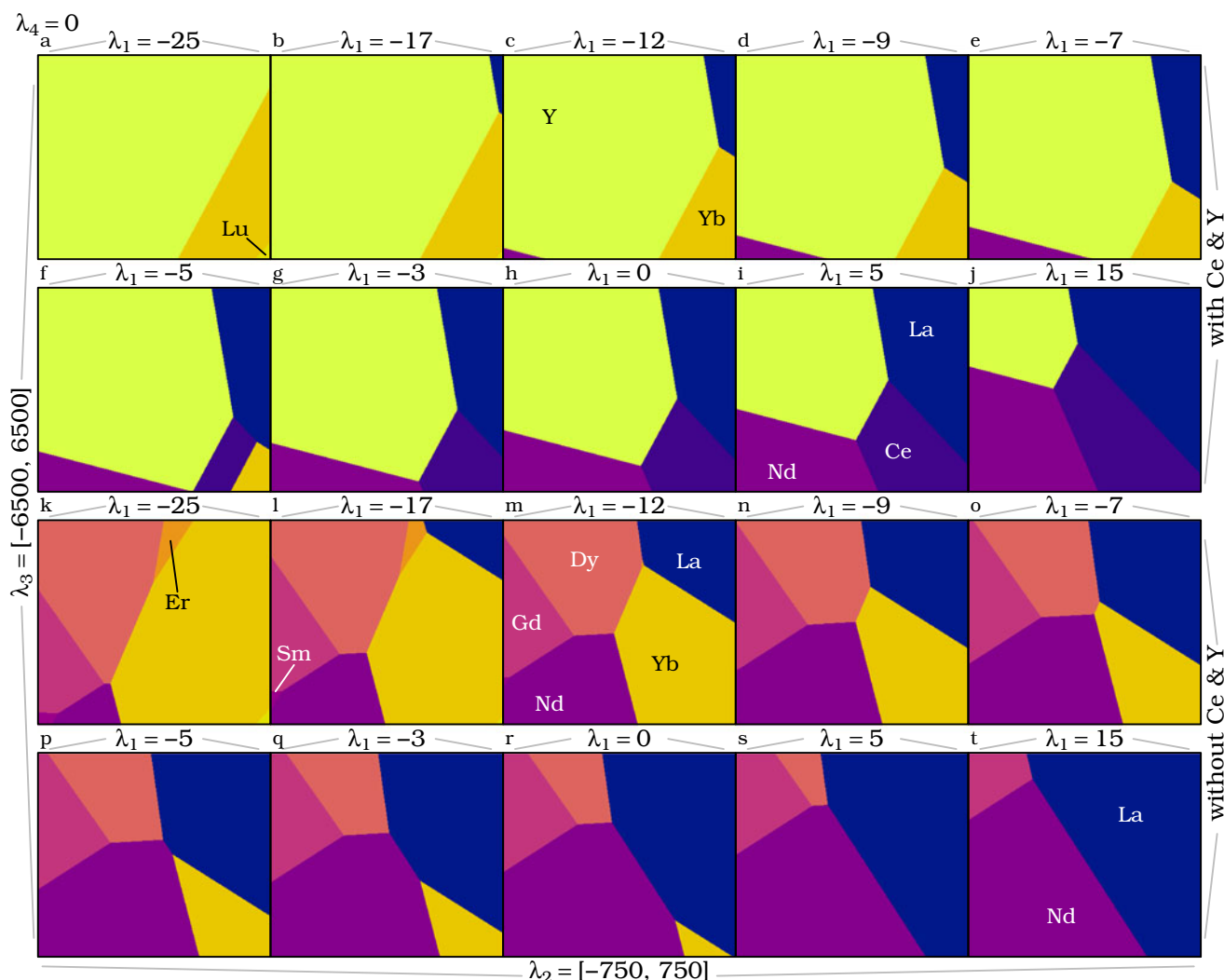


Fig. 3. A comparison between the dominant element of each pattern including Ce and Y (top two rows) and excluding Ce and Y (bottom two rows) with λ_4 fixed at 0. Colours indicate individual elements. Not all fields are annotated, but colours are consistent. A full colour key is available in the Supplementary materials. λ_1 to λ_3 are similar to Fig. 2.

The lower two rows in Fig. 3 *k–t* show the same calculation, but without Ce and Y. The area previously occupied by Ce is now shared between La and Nd, with the boundary between the two occurring at the centre of most panels. Rare earth element minerals tend to occur in REE-rich rocks which often include carbonatites and peralkaline rocks (Chakhmouradian and Zaitsev, 2012; Dostal, 2017; McLeod and Shaulis, 2018; Verplanck *et al.*, 2016). These rocks often have strongly negatively sloping REE patterns, which are represented by patterns with $\lambda_2 > 0$, well within the La field of Fig. 2, explaining the large diversity of La-dominated minerals (Krivovichev and Charykova, 2017).

The Ce–Y-absent plots (bottom half of Fig. 3) also show the potential for HREE-dominant minerals. The largest HREE field in most panels is the Yb field and indeed there are four known Yb minerals. The Dy fields reach the centre of most plots, suggesting that Dy-dominated minerals are likely to occur in Nature. However, none are yet known, probably because of the high abundance of Y in these minerals (see discussion below). Likewise, the Gd fields are significant and reach areas near the centre of the plots, but only one Gd mineral is known at present (Deliens

and Piret, 1982). Additionally, small Er and Sm fields occur in the $\lambda_1 = -25$ and $\lambda_1 = -17$ plots. No Er minerals are currently known. Surprisingly, even though the Sm fields occur in the lower left corners, there are two Sm minerals known. A possible reason is that these corners correspond to places where Y is less abundant (compare the positions of the Sm fields with the same positions in the top two rows of Fig. 3 *a–j*), thus merely requiring a small negative Y anomaly for Sm to predominate. Alternatively, the Er and Sm fields are enlarged when λ_4 deviates from zero. Fig. 4 shows an enlarged Er field at $\lambda_4 = -40,000$ and enlarged Sm field (along with Gd) at $\lambda_4 = 40,000$ that impinge on the geologically reasonable panel centres.

The REE appearing in Figs 3 and 4 correlate closely with the Oddo–Harkins rule. The plots contain mostly elements with even atomic numbers (Ce, Nd, Sm, Gd, Dy, Er and Yb). The only odd-numbered elements that reach dominance are La and Lu, which occur on opposite edges of the REE series. The primary reasons for La dominance were described above, but another reason is that both La and Lu are bounded by only one even-numbered REE (Ce and Yb, respectively) instead of two like all

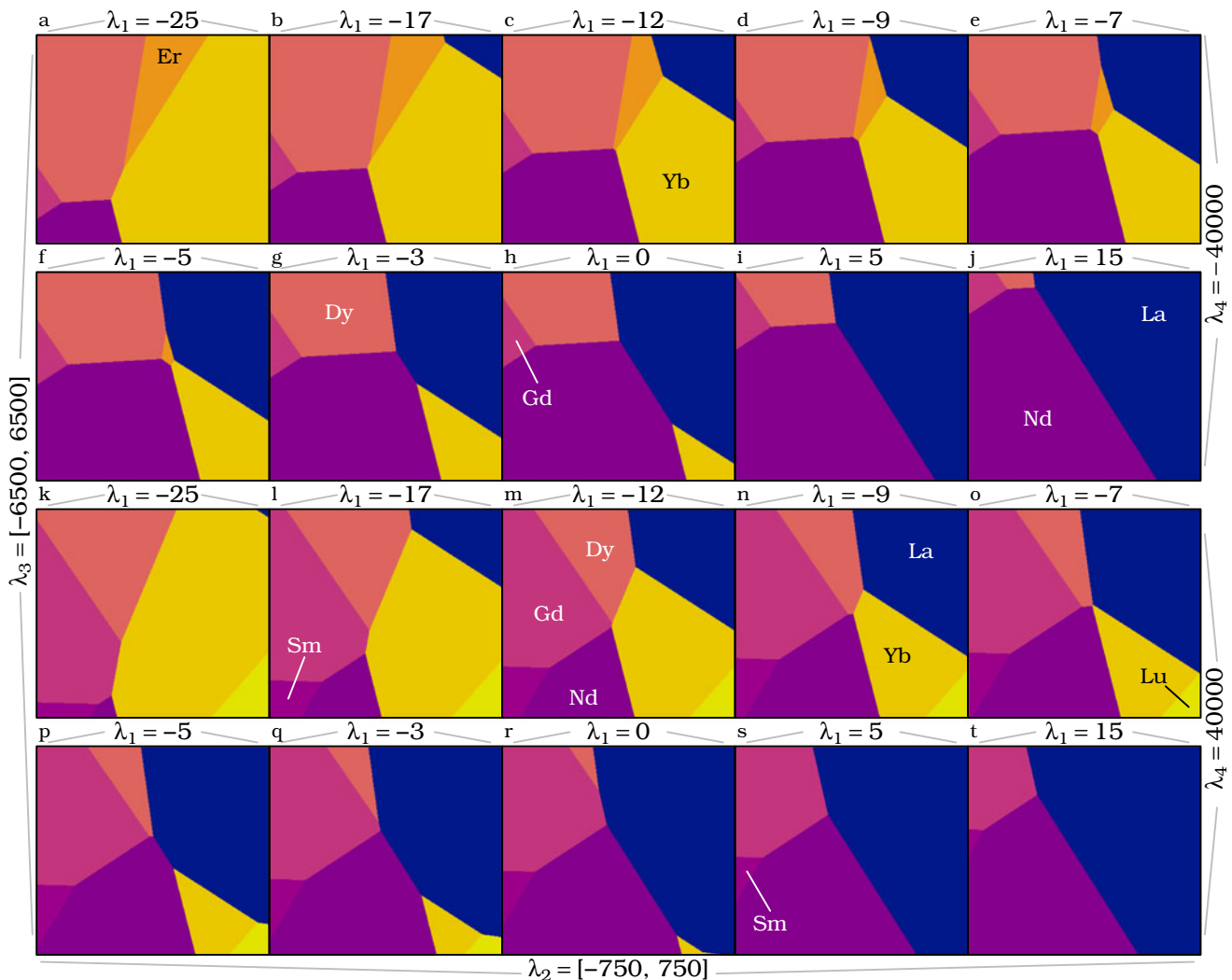


Fig. 4. A comparison between the dominant element for each pattern excluding Ce and Y. Construction of panels is similar to Fig. 3, with the top two rows showing $\lambda_4 = -40,000$ and the bottom two rows showing $\lambda_4 = 40,000$. Inclusion of Ce and Y results in panels almost identical to the top two rows of Fig. 3, which are not shown here.

other odd-numbered REE. Finally, Lu appears only on some plots at highly unrealistic $\lambda_2 \gg 0$ and $\lambda_3 \ll 0$, so it will never overtake the abundance of Yb for all practical purposes. The Oddo–Harkins rule is well demonstrated with Pr, which has the fourth largest crustal abundance of all lanthanides, and fifth when including Y. However, no predicted REE pattern contains Pr as the most abundant REE, even when excluding the neighbouring Ce, because Nd is much more abundant than Pr. It may be possible to concentrate Pr by fractionating it from the other REE by oxidation to Pr^{4+} , but hitherto only trace amounts of Pr^{4+} have been detected in terrestrial rocks (Anenburg *et al.*, 2020a).

Europium anomalies

The anomalous redox behaviour of Eu allows its concentration in Ca-rich minerals, most notably plagioclase and epidote (Anenburg *et al.*, 2015; Bédard, 2006; Bieseler *et al.*, 2018; Frei *et al.*, 2004; Rudnick, 1992; Schoneveld and O'Neill, 2019). It is possible to calculate the stage at which Eu becomes the most

abundant REE in a mineral by calculating the ratio between the most abundant REE and Eu. The result is the minimum positive Eu anomaly required for it to predominate. Generally, Eu anomalies are calculated using the geometric mean of the neighbouring elements by $\text{Eu}/\text{Eu}^* = \text{Eu}/\sqrt{\text{Sm} \times \text{Gd}}$, however this can lead to errors in patterns with strong curvature at Eu (see Fig. 5). Here, Eu anomalies are calculated relative to the expected Eu from the polynomial fit.

Figure 6 shows the Eu anomaly required for it to predominate at different λ values. As above, the removal of Ce and Y allows for smaller Eu anomalies to suffice. The greatest influence comes from λ_2 , which reduces the required anomaly as it becomes more negative. This is expected as patterns with negative λ_2 are parabolic with maxima precisely at Eu. The required Eu anomalies close to the plot centres are often in the range of 5 to 10, which is a reasonable value often seen in nature. Prolonged surface weathering often leads to concentration of REE, and it is probable that Eu-dominated minerals will form in strongly weathered anorthosites or epidiosites (e.g. Banerjee and Chakrabarti, 2018).

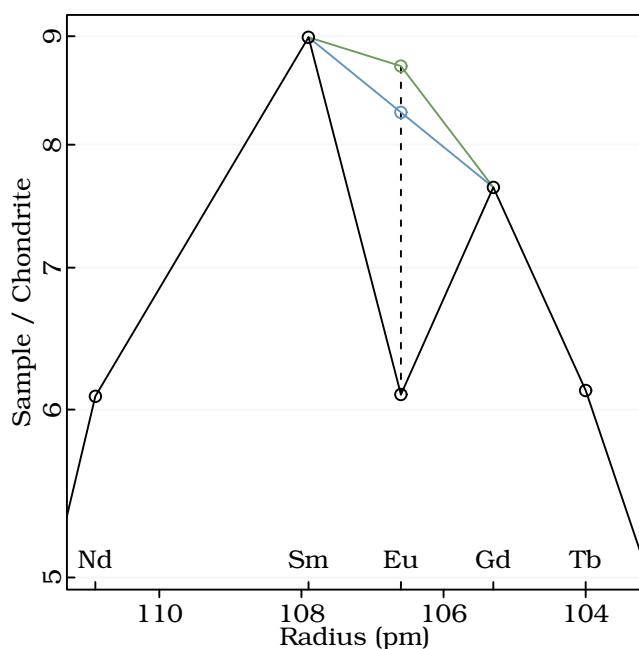


Fig. 5. A Nd-Tb portion of a pattern generated with $\lambda_0=1$, $\lambda_1=0$, $\lambda_2=-300$, and $\lambda_3=-1000$ and no Eu anomaly (green line). However, an attempt to calculate the anomaly using interpolation of the neighbouring elements (blue line) leads to $\text{Eu}/\text{Eu}^* = \text{Eu}/\sqrt{\text{Sm} \times \text{Gd}} = 1.05$, suggesting a small positive, yet spurious, Eu anomaly.

Comparison with natural minerals

Rare earth element patterns and polynomial fits calculated from data available for four Yb minerals and two Sm minerals are given in Fig. 7. The polynomial fits to the Yb minerals reasonably agree with the observed patterns. Likewise, projection of their coefficients into $\lambda_2 - \lambda_3$ space shows they all plot within their respective Yb fields (marked by similarly coloured lines). In contrast, the polynomial fits to the Sm minerals fail to reproduce the high Sm contents. Moreover, their projections plot outside of the Sm-dominant fields in $\lambda_2 - \lambda_3$ space. This could result from analytical challenges as the REE are measured by wavelength-dispersive spectroscopy, a method which suffers from peak overlaps and requires careful calibration and matrix corrections. Analytical problems aside, this could indicate an additional geochemical fractionation process not captured by the shape coefficient model. Such processes are common in low-temperature environments, some examples being the seemingly hydrothermal texture shown by the florencite-(Sm) domains described by Repina *et al.* (2014). This method does not capture variability caused by the tetrad effect, which may become important at similar low temperatures or unusual fluid chemistries (Irber, 1999; Monecke *et al.*, 2002).

Mineral evolution and nomenclature

There are fewer minerals with essential REE than expected according to their crustal abundance (Christy, 2015; Hazen *et al.*, 2015a; Higgins and Smith, 2010; Krivovichev *et al.*, 2018; Rieder, 2016). The Ca ionic radius is close to that of Pr (112 pm and 112.6 pm, respectively, Shannon, 1976), and consequently the LREE are often dispersed as trace elements in Ca-rich minerals. Minerals with smaller Ca sites (such as clinopyroxenes) or with rigid structures will strongly partition HREE relative to

LREE (most notably garnet and zircon, Dubacq and Plunder, 2018) provided that charge balance is achieved. As a result, REE rarely form minerals of their own and instead occur as trace elements in other minerals. Even when REE do form their own minerals, they are dominated mostly by Ce and Y, with the less abundant REE incorporated as subordinate components in solid solution (i.e. they ‘mimic’ Ce and Y, Hazen *et al.*, 2015b). No single mineral is capable of isolating a single trivalent REE, but instead incorporate the entire REE series to various degrees. Nonetheless, some minerals have crystal chemical constraints that lead to preferential uptake of a narrower REE range, leading to exceptional concentration of a certain subset relative to the others (Mitchell *et al.*, 1994). Guidelines published by the International Mineralogical Association Commission on New Minerals, Nomenclature and Classification (IMA-CNMNC) require names of minerals containing essential REE to have a suffix denoting the most abundant REE (Hatert *et al.*, 2013; Nickel and Grice, 1998). These suffixes are known as ‘Levinson’ suffixes (Bayliss and Levinson, 1988; Levinson, 1966). Insofar as nomenclature is inevitably subjective, it could be hard to justify naming a new mineral species. For example, instances of florencite-(Sm) described by Repina *et al.* (2011) are not individual grains, but rather Sm-dominated thin growth zones inside florencite-(Ce). Hazen (2019) argued that the diversity of REE minerals is an artificial construct by the IMA-CNMNC mineral names rules. He states: “...these split species represent a single natural kind with one stability field that incorporates yttrium and a range of light and heavy REE and thus one paragenetic mode” (Hazen, 2019). However, this statement misses a great deal of nuance in REE geochemistry. Indeed, two minerals with similar REE contents but one containing $\text{La}/\text{Ce}=0.95$ and the other $\text{La}/\text{Ce}=1.05$ will share similar thermodynamic properties and virtually indistinguishable stability fields, even though they will have different mineral names. This is not the case for elements that are farther apart. For example, the thermodynamic properties of bastnäsäsite-(Ce) and bastnäsäsite-(Y), or hingganite-(Ce) and hingganite-(Yb) are probably sufficiently different to justify their own mineral species (e.g. Miyawaki and Nakai, 1996)—probably more than zircon and hafnon are justified.

The rarity of REE minerals dominated by Sm, Gd, Dy, Er or Yb is a direct consequence of the composition (X) component of the Hazen and Ausubel (2016) first criterion for mineral rarity: $P-T-X$ range. As shown above, the formation of most Y-absent HREE-dominated species require a negative Y anomaly, and a negative Ce anomaly allows greater dominance of La and Nd. These anomalies require distinct geochemical conditions, either F-rich fluids (Loges *et al.*, 2013) or coexistence of fluorite for Y anomalies (Chebotarev *et al.*, 2019), and oxidising conditions coupled with low temperatures for Ce anomalies (Anenburg *et al.*, 2018; Burnham and Berry, 2014; Sørensen, 1976). The small Sm-dominant zones inside florencite grains reported by Repina *et al.* (2011) require exceptional formation conditions (Repina *et al.*, 2014). Therefore, ‘one paragenetic mode’ cannot account for the entire diversity observed in REE mineral name suffixes, and they do not represent ‘a single natural kind’ (also remembering that the ‘natural kind’ concept and mineralogy are incompatible; Santana, 2019). The processes that lead to one REE predominating over another are real fractionation processes occurring in Nature. It follows that identification of REE minerals with uncommon dominant elements expand our recognition of attainable extremes in terrestrial geochemical fractionation processes (Hazen and Ausubel, 2016).

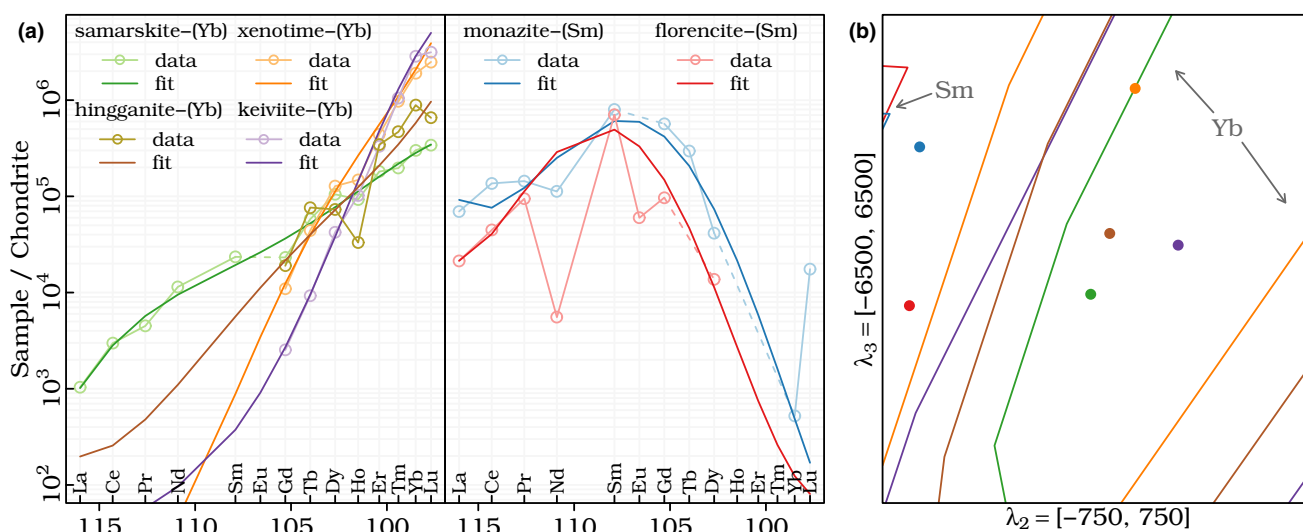


Fig. 7. (a) Literature data for REE minerals and their corresponding polynomial fits. The macro provided by O'Neill (2016) requires data for Ce or La, which was not available for all minerals. See Supplementary material for resulting λ values, information on assumed values, and discarded values of poor data quality. (b) Projection of λ values used to construct the patterns in (a) to λ_2 - λ_3 space. Coloured lines indicate the field boundaries for dominant Sm (red and blue) and Yb (all others). Data sources: Masau *et al.* (2002), Repina *et al.* (2011), Voloshin *et al.* (1984), Voloshin *et al.* (1983), Simmons *et al.* (2006) and Buck *et al.* (1999).

demonstrates that once HREE mineral chemistry is looked at beyond Y, a greater diversity is discovered. It is possible that many more REE minerals—which reflect real geochemical fractionation processes—will be ‘rediscovered’ if Y is removed from Levinson suffixes. Furthermore, future advances in analytical methods are likely to reveal small scale heterogeneities in which unusual REE will predominate (Cook *et al.*, 2017).

Supplementary material. To view supplementary material for this article, please visit <https://doi.org/10.1180/mgm.2020.70>

Acknowledgements. Hugh O'Neill is thanked for thought-provoking discussions. Stuart Mills is thanked for his editorial handling.

Data. All data and figures in this article were generated using R 4.0.2 from the R script ‘*REEpatterns.R*’ available in the Supplementary materials.

References

- Alekseev V.I. and Marin Y.B. (2014) A tribute to Nicolai Pavlovich Yushkin, one of the discoverers of chernovite. Chernovite-(Y) and other arsenic minerals in rare-metal granites and greisens of the Far East. *Geology of Ore Deposits*, **55**, 601–606. <https://doi.org/10.1134/s1075701513070039>
- Anenburg M., Katzir Y., Rhede D., Jöns N. and Bach W. (2015) Rare earth element evolution and migration in plagiogranites: a record preserved in epidote and allanite of the Troodos ophiolite. *Contributions to Mineralogy and Petrology*, **169**, 25. <https://doi.org/10.1007/s00410-015-1114-y>
- Anenburg M., Burnham A.D. and Mavrogenes J.A. (2018) REE redistribution textures in altered fluorapatite: Symplectites, veins and phosphate-silicate-carbonate assemblages from the Nolans Bore P-REE-Th deposit, NT, Australia. *The Canadian Mineralogist*, **56**, 331–354. <https://doi.org/10.3749/canmin.1700038>
- Anenburg M., Burnham A.D. and Hamilton J.L. (2020a) Quadrivalent praseodymium in planetary materials. *American Mineralogist*, **105**, <https://doi.org/10.2138/am-2020-7325>
- Anenburg M., Mavrogenes J.A. and Bennett V.C. (2020b) The fluorapatite P-REE-Th vein deposit at Nolans Bore: Genesis by carbonatite metasomatism. *Journal of Petrology*, **61**, ega003 <https://doi.org/10.1093/petrology/egaa003>
- Balarum V. (2019) Rare earth elements: A review of applications, occurrence, exploration, analysis, recycling, and environmental impact. *Geoscience Frontiers*, **10**, 1285–1303. <https://doi.org/10.1016/j.gsf.2018.12.005>
- Banerjee A. and Chakrabarti R. (2018) Large Ca stable isotopic ($\delta^{44/40}\text{Ca}$) variation in a hand-specimen sized spheroidally weathered diabase due to selective weathering of clinopyroxene and plagioclase. *Chemical Geology*, **483**, 295–303. <https://doi.org/10.1016/j.chemgeo.2018.02.031>
- Bayliss P. and Levinson A.A. (1988) A system of nomenclature for rare-earth mineral species: Revision and extension. *American Mineralogist*, **73**, 422–423.
- Bédard J.H. (2006) Trace element partitioning in plagioclase feldspar. *Geochimica et Cosmochimica Acta*, **70**, 3717–3742. <https://doi.org/10.1016/j.gca.2006.05.003>
- Bédard J.H. (2014) Parameterizations of calcic clinopyroxene — Melt trace element partition coefficients. *Geochemistry, Geophysics, Geosystems*, **15**, 303–336. <https://doi.org/10.1002/2013gc005112>
- Bieseler B., Diehl A., Jöns N., Lucassen F. and Bach W. (2018) Constraints on cooling of the lower ocean crust from epidote veins in the Wadi Gideah section, Oman Ophiolite. *Geochemistry, Geophysics, Geosystems*, **19**, 4195–4217. <https://doi.org/10.1029/2018gc007679>
- Buck H.M., Cooper M.A., Černý P., Grice J.D. and Hawthorne F.C. (1999) Xenotime-(Yb), YbPO_4 , a new mineral species from the Shatford Lake pegmatite group, southeastern Manitoba, Canada. *The Canadian Mineralogist*, **37**, 1303–1306.
- Burnham A.D. and Berry A.J. (2014) The effect of oxygen fugacity, melt composition, temperature and pressure on the oxidation state of cerium in silicate melts. *Chemical Geology*, **366**, 52–60. <https://doi.org/10.1016/j.chemgeo.2013.12.015>
- Chakhmouradian A.R. and Zaitsev A.N. (2012) Rare earth mineralization in igneous rocks: sources and processes. *Elements*, **8**, 347–353. <https://doi.org/10.2113/gselements.8.5.347>
- Chebotaev D.A., Veksler I.V., Wohlgemuth-Ueberwasser C., Doroshkevich A.G. and Koch-Müller M. (2019) Experimental study of trace element distribution between calcite, fluorite and carbonatitic melt in the system $\text{CaCO}_3 + \text{CaF}_2 + \text{Na}_2\text{CO}_3 \pm \text{Ca}_3(\text{PO}_4)_2$ at 100 MPa. *Contributions to Mineralogy and Petrology*, **174**, 4. <https://doi.org/10.1007/s00410-018-1530-x>
- Chesson T. and Schelter E.J. (2019) Rare earth elements: Mendeleev’s bane, modern marvels. *Science*, **363**, 489–493. <https://doi.org/10.1126/science.aau7628>

- Christy A.G. (2015) Causes of anomalous mineralogical diversity in the Periodic Table. *Mineralogical Magazine*, **79**, 33–49. <https://doi.org/10.1180/minmag.2015.079.1.04>
- Cook N., Ciobanu C., Ehrig K., Slattery A., Verdugo-Ihl M., Courtney-Davies L. and Gao W. (2017) Advances and opportunities in ore mineralogy. *Minerals*, **7**, 233. <https://doi.org/10.3390/min7120233>
- Coryell C.D., Chase J.W. and Winchester J.W. (1963) A procedure for geochemical interpretation of terrestrial rare-earth abundance patterns. *Journal of Geophysical Research*, **68**, 559–566. <https://doi.org/10.1029/JZ068i002p00559>
- Davidson J., Turner S. and Plank T. (2013) Dy/Dy*: Variations arising from mantle sources and petrogenetic processes. *Journal of Petrology*, **54**, 525–537. <https://doi.org/10.1093/ptrology/egs076>
- Deliens M. and Piret P. (1982) Bijvoetite et lepersonnite, carbonates hydratés d'uranyle et de terres rares de Shinkolobwe, Zaïre. *The Canadian Mineralogist*, **20**, 231–238.
- Dostal J. (2017) Rare earth element deposits of alkaline igneous rocks. *Resources*, **6**, 34. <https://doi.org/10.3390/resources6030034>
- Dubacq B. and Plunder A. (2018) Controls on trace element distribution in oxides and silicates. *Journal of Petrology*, **59**, 233–256. <https://doi.org/10.1093/ptrology/egy027>
- Ferru G., Reinhart B., Bera M.K., Olvera de la Cruz M., Qiao B. and Ellis R.J. (2016) The lanthanide contraction beyond coordination chemistry. *Chemistry – A European Journal*, **22**, 6899–8904. <https://doi.org/10.1002/chem.201601032>
- Frei D., Liebscher A., Franz G. and Dulski P. (2004) Trace element geochemistry of epidote minerals. Pp. 553–606 in: *Epidotes*. (A. Liebscher and G. Franz, editors). Reviews in Mineralogy and Geochemistry, **56**. Mineralogical Society of America and the Geochemical Society, Washington, DC. <https://doi.org/10.2138/gsrmg.56.1.553>
- Harkins W.D. (1917) The evolution of the elements and the stability of complex atoms. I. A new periodic system which shows a relation between the abundance of the elements and the structure of the nuclei of atoms. *Journal of the American Chemical Society*, **39**, 856–879. <https://doi.org/10.1021/ja02250a002>
- Hatert F., Mills S.J., Pasero M. and Williams P.A. (2013) CNMNC guidelines for the use of suffixes and prefixes in mineral nomenclature and for the preservation of historical names. *European Journal of Mineralogy*, **25**, 113–115. <https://doi.org/10.1127/0935-1221/2013/0025-2267>
- Hazen R.M. (2014) Data-driven abductive discovery in mineralogy. *American Mineralogist*, **99**, 2165–2170. <https://doi.org/10.2138/am-2014-4895>
- Hazen R.M. (2019) An evolutionary system of mineralogy: Proposal for a classification of planetary materials based on natural kind clustering. *American Mineralogist*, **104**, 810–816. <https://doi.org/10.2138/am-2019-6709CCBYNCND>
- Hazen R.M. and Ausubel J.H. (2016) On the nature and significance of rarity in mineralogy. *American Mineralogist*, **101**, 1245–1251. <https://doi.org/10.2138/am-2016-5601CCBY>
- Hazen R.M., Grew E.S., Downs R.T., Golden J. and Hystad G. (2015a) Mineral ecology: chance and necessity in the mineral diversity of terrestrial planets. *The Canadian Mineralogist*, **53**, 295–324. <https://doi.org/10.3749/canmin.1400086>
- Hazen R.M., Hystad G., Downs R.T., Golden J.J., Pires A.J. and Grew E.S. (2015b) Earth's "missing" minerals. *American Mineralogist*, **100**, 2344–2347. <https://doi.org/10.2138/am-2015-5417>
- Hazen R.M., Hummer D.R., Hystad G., Downs R.T. and Golden J.J. (2016) Carbon mineral ecology: Predicting the undiscovered minerals of carbon. *American Mineralogist*, **101**, 889–906. <https://doi.org/10.2138/am-2016-5546>
- Higgins M.D. and Smith D.G.W. (2010) A census of mineral species in 2010. *Elements*, **6**, 346.
- Irber W. (1999) The lanthanide tetrad effect and its correlation with K/Rb, Eu/Eu*, Sr/Eu, Y/Ho and Zr/Hf of evolving peraluminous granite suites. *Geochimica et Cosmochimica Acta*, **63**, 489–508. [https://doi.org/10.1016/S0016-7037\(99\)00027-7](https://doi.org/10.1016/S0016-7037(99)00027-7)
- Krivovichev V.G. and Charykova M.V. (2017) Mineral systems, their types and distribution in nature. I. Khibiny, Lovozero and the Mont Saint-Hilaire. *Geology of Ore Deposits*, **58**, 551–558. <https://doi.org/10.1134/S1075701516070059>
- Krivovichev V.G., Charykova M.V. and Krivovichev S.V. (2018) The concept of mineral systems and its application to the study of mineral diversity and evolution. *European Journal of Mineralogy*, **30**, 219–230. <https://doi.org/10.1127/ejm/2018/0030-2699>
- Kuroda P.K. (1982) Elements 43 and 61 in nature. Pp. 15–29 in: *The Origin of the Chemical Elements and the Oklo Phenomenon*. Springer, Berlin. https://doi.org/10.1007/978-3-642-68667-2_3
- Levinson A.A. (1966) A system of nomenclature for rare-earth minerals. *American Mineralogist*, **51**, 152–158.
- Loges A., Migdisov A.A., Wagner T., Williams-Jones A.E. and Markl G. (2013) An experimental study of the aqueous solubility and speciation of Y(III) fluoride at temperatures up to 250 °C. *Geochimica et Cosmochimica Acta*, **123**, 403–415. <https://doi.org/10.1016/j.gca.2013.07.031>
- Masau M., Černý P., Cooper M.A., Chapman R. and Grice J.D. (2002) Monazite-(Sm), a new member of the monazite group from the Annie Claim #3 granitic pegmatite, Southeastern Manitoba. *The Canadian Mineralogist*, **40**, 1649–1655. <https://doi.org/10.2113/gscanmin.40.6.1649>
- McLeod C. and Shaulis B. (2018) Rare earth elements in planetary crusts: Insights from chemically evolved igneous suites on Earth and the Moon. *Minerals*, **8**, 455. <https://doi.org/10.3390/min8100455>
- Minami M. and Masuda A. (1997) Approximate estimation of the degree of lanthanide tetrad effect from the data potentially involving all lanthanides. *Geochemical Journal*, **31**, 125–133.
- Mitchell R.H., Novgorodova M.I. and Semenov E.I. (1994) Chemical composition of minerals, crystallochemical constraints and the nature of impurities. Pp. 2–12 in: *Advanced Mineralogy, Volume 1: Composition, Structure, and Properties of Mineral Matter: Concepts, Results and Problems* (A.S. Marfunin, editor). Springer, Berlin. https://doi.org/10.1007/978-3-642-78523-8_1
- Miyawaki R. and Nakai I. (1996) Crystal chemical aspects of rare earth minerals. Pp. 21–40 in: *Rare Earth Minerals, Chemistry, Origin and Ore Deposits* (A.P. Jones, F. Wall and C.T. Williams, editors). Chapman and Hall, London.
- Monecke T., Kempe U., Monecke J., Sala M. and Wolf D. (2002) Tetrad effect in rare earth element distribution patterns: a method of quantification with application to rock and mineral samples from granite-related rare metal deposits. *Geochimica et Cosmochimica Acta*, **66**, 1185–1196. [https://doi.org/10.1016/S0016-7037\(01\)00849-3](https://doi.org/10.1016/S0016-7037(01)00849-3)
- Nickel E.H. and Grice J.D. (1998) The IMA Commission on New Minerals and Mineral Names: procedures and guidelines on mineral nomenclature, 1998. *The Canadian Mineralogist*, **36**, 913–926.
- Ondrejka M., Uher P., Pršek J. and Ozdin D. (2007) Arsenian monazite-(Ce) and xenotime-(Y), REE arsenates and carbonates from the Tisovec-Rejkovo rhyolite, Western Carpathians, Slovakia: Composition and substitutions in the (REE,Y)XO₄ system (X=P, As, Si, Nb, S). *Lithos*, **95**, 116–129. <https://doi.org/10.1016/j.lithos.2006.07.019>
- O'Neill H.S.C. (2016) The smoothness and shapes of chondrite-normalized rare earth element patterns in basalts. *Journal of Petrology*, **57**, 1463–1508. <https://doi.org/10.1093/ptrology/egw047>
- Pack A., Russell S.S., Shelley J.M.G. and van Zuilen M. (2007) Geo- and cosmochemistry of the twin elements yttrium and holmium. *Geochimica et Cosmochimica Acta*, **71**, 4592–4608. <https://doi.org/10.1016/j.gca.2007.07.010>
- Palme H., Lodders K. and Jones A. (2014) Solar system abundances of the elements. Pp. 15–36 in: *Treatise on Geochemistry (Second Edition), Volume 2: Planets, Asteroids, Comets and The Solar System* (A.M. Davis, editor). Elsevier, Amsterdam. <https://doi.org/10.1016/B978-0-08-095975-7.00118-2>
- Raymond K.N., Wellman D.L., Sgarlata C. and Hill A.P. (2010) Curvature of the lanthanide contraction: An explanation. *Comptes Rendus Chimie*, **13**, 849–852. <https://doi.org/10.1016/j.crci.2010.03.034>
- Repina S.A., Popova V.I., Churin E.I., Belogub E.V. and Khiller V.V. (2011) Florencite-(Sm)—(Sm,Nd)Al₃(PO₄)₂(OH)₆: A new mineral species of the alunite-jarosite group from the subpolar urals. *Geology of Ore Deposits*, **53**, 564–574. <https://doi.org/10.1134/S1075701511070191>
- Repina S.A., Khiller V.V. and Makagonov E.P. (2014) Microheterogeneity of crystal growth zones as a result of REE fractionation. *Geochemistry International*, **52**, 1057–1071. <https://doi.org/10.1134/S0016702914100085>

- Rieder M. (2016) The mineralogical system: Can global plots teach us something new? *Mineralogical Magazine*, **80**, 239–248. <https://doi.org/10.1180/minmag.2016.080.012>
- Rudnick R.L. (1992) Restites, Eu anomalies and the lower continental crust. *Geochimica et Cosmochimica Acta*, **56**, 963–970. [https://doi.org/10.1016/0016-7037\(92\)90040-p](https://doi.org/10.1016/0016-7037(92)90040-p)
- Rudnick R.L. and Gao S. (2014) Composition of the continental crust. Pp. 1–51 in: *Treatise on Geochemistry (Second Edition), Volume 4: The Crust* (R.L. Rudnick, editor). Elsevier, Amsterdam. <https://doi.org/10.1016/b978-0-08-095975-7.00301-6>
- Santana C. (2019) Mineral misbehavior: why mineralogists don't deal in natural kinds. *Foundations of Chemistry*, **21**, 333–343. <https://doi.org/10.1007/s10698-019-09338-3>
- Savel'yeva V.B., Bazarova E.P., Khromova E.A. and Kanakin S.V. (2019) REE minerals in the rocks of the Katugin rare metal deposit, East Transbaikalia: Behavior of lanthanides and Y during crystallization of an F-saturated apatitic melt. *Geology of Ore Deposits*, **60**, 643–657. <https://doi.org/10.1134/s1075701518080093>
- Schoneveld L. and O'Neill H.S.C. (2019) The influence of melt composition on the partitioning of trace elements between anorthite and silicate melt. *Contributions to Mineralogy and Petrology*, **174**, 13. <https://doi.org/10.1007/s00410-019-1548-8>
- Seitz M., Oliver A.G. and Raymond K.N. (2007) The lanthanide contraction revisited. *Journal of the American Chemical Society*, **129**, 11153–11160. <https://doi.org/10.1021/ja072750f>
- Shannon R.D. (1976) Revised effective ionic radii and systematic studies of interatomic distances in halides and chalcogenides. *Acta Crystallographica A*, **32**, 751–767. <https://doi.org/10.1107/s0567739476001551>
- Simmons W.B., Hanson S.L. and Falster A.U. (2006) Samarskite-(Yb): A new species of the samarskite group from the Little Patsy pegmatite, Jefferson County, Colorado. *The Canadian Mineralogist*, **44**, 1119–1125. <https://doi.org/10.2113/gscanmin.44.5.1119>
- Sørensen O.T. (1976) Thermodynamic studies of the phase relationships of nonstoichiometric cerium oxides at higher temperatures. *Journal of Solid State Chemistry*, **18**, 217–233. [https://doi.org/10.1016/0022-4596\(76\)90099-2](https://doi.org/10.1016/0022-4596(76)90099-2)
- Taylor S.R. (1962) Meteoritic and terrestrial rare earth abundance patterns. *Geochimica et Cosmochimica Acta*, **26**, 81–88. [https://doi.org/10.1016/0016-7037\(62\)90007-8](https://doi.org/10.1016/0016-7037(62)90007-8)
- Verplanck P.L., Mariano A.N. and Mariano Jr. A. (2016) Rare earth element ore geology of carbonatites. Pp. 5–32 in: *Rare Earth and Critical Elements in Ore Deposits* (P.L. Verplanck and M.W. Hitzman, editors). Society of Economic Geologists, Littleton, Colorado, USA. <https://doi.org/10.5382/Rev.18.01>
- Voloshin A.V., Pakhomovsky Y.A. and Tyusheva F.N. (1983) Keiviite Yb₂Si₂O₇, a new ytterbium silicate from amazonitic pegmatites of the Kola Peninsula. *Mineralog Zhurnal*, **5**, 94–99.
- Voloshin A.V., Pakhomovskii Y.A., Men'shikov Y.P., Povarennykh A.S., Matvinenko E.N. and Yakubovich O.V. (1984) Hingganite-(Yb), a new mineral from Amazonite pegmatite of the Kola Peninsula. *International Geology Review*, **26**, 60–63. <https://doi.org/10.1080/00206818409452995>
- Williams M.J., Schoneveld L., Mao Y., Klump J., Gosses J., Dalton H., Bath A. and Barnes S. (2020) Pyrolite: Python for geochemistry. *Journal of Open Source Software*, **5**, 2314. <https://doi.org/10.21105/joss.02314>

Appendix

ALambdaR is an online interactive app developed in R that generates REE patterns from input describing the REE pattern shape, available at <https://lambda-r.rses.anu.edu.au/lambda-r/>. The app takes numerical input of λ_0 to λ_4 , Eu and Ce anomalies and Y/Ho ratio. It generates REE abundances from which it shows a normalised REE pattern according to a normalisation scheme selected by the user. A pie chart showing the relative properties of all REE is also given. It is possible to export the plots in either pdf (vector) or png (raster) formats, and export the data in comma separated values (csv) format. The app also allows upload of files in csv format containing multiple combinations of λ_0 to λ_4 , and it generates a downloadable file containing the resulting REE abundances in $\mu\text{g g}^{-1}$ units. Future versions will include tetrad effects for a more comprehensive REE pattern generation functionality (e.g. Irber, 1999; Minami and Masuda, 1997; Monecke *et al.*, 2002).

For calculating a REE pattern using λ shape coefficients, the app uses a matrix F that includes all f_n values:

$$F = \begin{pmatrix} f_{\text{La},1} & \cdots & f_{\text{La},4} \\ f_{\text{Ce},1} & \cdots & f_{\text{Ce},4} \\ \vdots & \ddots & \vdots \\ f_{\text{Lu},1} & \cdots & f_{\text{Lu},4} \end{pmatrix} = \begin{pmatrix} 0.1052 & \cdots & 8.29 \times 10^{-6} \\ 0.0882 & \cdots & -7.16 \times 10^{-6} \\ \vdots & \ddots & \vdots \\ -0.0778 & \cdots & 9.41 \times 10^{-6} \end{pmatrix}$$

The full set of values is available in O'Neill (2016) or in the Supplementary code. Each REE pattern can be described as a combination of λ values, and a column vector is defined:

$$\vec{\lambda} = \begin{pmatrix} \lambda_1 \\ \lambda_2 \\ \lambda_3 \\ \lambda_4 \end{pmatrix}$$

The REE contents for each corresponding $\vec{\lambda}$ can be calculated using matrix multiplication:

$$\overrightarrow{\ln\left(\frac{[\text{REE}]}{[\text{REE}]_{\text{CI}}}\right)} = F\vec{\lambda} + \lambda_0.$$

The choice of the logarithm base does not change the pattern shape. However, in some cases it might be desirable to transform the values to base 10 which is achieved via:

$$\overrightarrow{\log\left(\frac{[\text{REE}]}{[\text{REE}]_{\text{CI}}}\right)} = \log e \times \overrightarrow{\ln\left(\frac{[\text{REE}]}{[\text{REE}]_{\text{CI}}}\right)}$$

If required, concentration values in $\mu\text{g g}^{-1}$ are calculated using:

$$\overrightarrow{[\text{REE}]} = \vec{C} \cdot e^{\overrightarrow{\ln\left(\frac{[\text{REE}]}{[\text{REE}]_{\text{CI}}}\right)}} = \vec{C} \cdot 10^{\overrightarrow{\log\left(\frac{[\text{REE}]}{[\text{REE}]_{\text{CI}}}\right)}}$$

Where \vec{C} is a vector of CI values from O'Neill (2016).